Enhancing aqueous carbonation of calcium silicate through acid and base pretreatments with implications for efficient carbon mineralization

Hang Zhai,[*] Qiyuan Chen, Mehmet Yilmaz, and Bu Wang[*]

Department of Civil and Environmental Engineering, University of Wisconsin-Madison, Madison, Wisconsin 53706, United States

[*]**To whom correspondence should be addressed.**

Hang Zhai

Department of Civil and Environmental

Engineering, University of Wisconsin-Madison, Madison, Wisconsin 53706, United States;

orcid.org/0000-0002-8161-448X;

Email: hzhai25@wisc.edu

Bu Wang

Department of Civil and Environmental

Engineering, University of Wisconsin-Madison, Madison, Wisconsin 53706, United States;

orcid.org/0000-0002-9294-0918;

Email: bu.wang@wisc.edu

ABSTRACT: Carbon dioxide (CO_2) mineralization based on aqueous carbonation of alkaline earth silicate minerals is a promising route towards large scale carbon removal. Traditional aqueous carbonation methods largely adopt acidification-based approaches, e.g., using concentrated/pressurized CO_2 or acidic media, to accelerate mineral dissolution and carbonation. In this study, we investigated aqueous carbonation under basic conditions using amorphous calcium silicate (CS) as an example system. We designed and tested three distinctive pretreatments routes to evaluate the effect of intermediate phases formed under different pH conditions on aqueous carbonation. Pretreating CS with high concentrations (100 mM) of HCl (Route I) or NaOH (Route II and III) enhanced their carbonation degrees. However, NaOH pretreatment overall yielded higher carbonation degrees than the HCl pretreatment, with the highest carbonation degree achieved through Route III, where an extra step is taken after the NaOH pretreatment to remove the solution containing dissolved silica prior to carbonation. The HCl and NaOH pretreatments formed different intermediate silica products on the CS surface. Silica precipitated from the HCl pretreatment had minimal effect on the carbonation degree. The Ca-rich intermediate phases (CIP) formed from the NaOH treatment, on the other hand, can be readily carbonated. In contrast to commonly utilized acid leaching approach, inducing the formation readily carbonatable CIP with basic conditions offers a more promising route to accelerate aqueous carbonation, as it can mitigate the need for costly pH swing and high-concentration/pressurized CO_2. The key to aqueous carbonation under basic conditions, as suggested by this study, is the control of aqueous silica species that have a suppressing effect on carbonation. Overall, this study highlights the critical needs for investigations of aqueous mineral carbonation in a broader pH region.

KEY WORDS: CO_2 mineralization, aqueous carbonation, calcium silicate, coupled dissolution-reprecipitation, secondary silicates.

SYNOPSIS: This study reveals a technology of CO_2 mineralization using acid or base-pretreated silicate minerals with the associated analyses of intermediate products after the pretreatments and impacts of silicon-byproducts during carbonation, which have strong

implications in improving the process efficiency and economics.

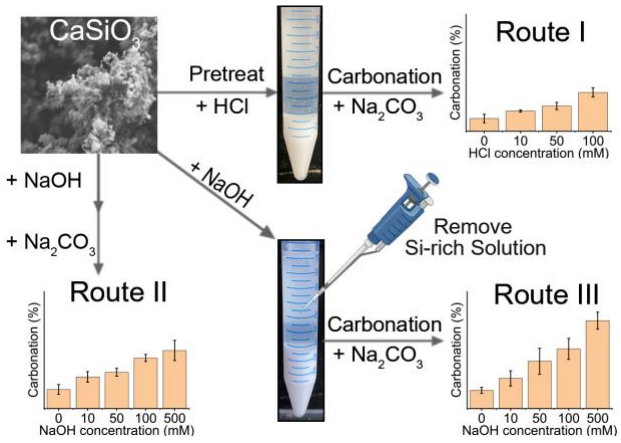

TOC

INTRODUCTION.

The continuing growth of the atmospheric carbon dioxide (CO_2) concentration is posing a risk of missing the climate targets.[1] In pathways towards rapid reduction of the CO_2 level, large scale carbon capture and storage (CCS) become almost indispensable.[2–4] As one of a handful of scalable options to durably store CO_2 away from the atmosphere, ex situ mineralization, wherein captured CO_2 are reacted with surficial Ca-, Mg-, or Fe-bearing minerals, such as wollastonite ($CaSiO_3$),[5] forsterite (Mg_2SiO_4),[6] fayalite (Fe_2SiO_4),[7] and phlogopite ($KMg_3(AlSi_3O_{10})(F, OH)_2$)[8] to form solid carbonates, has attracted significant attention. Comparing to in situ mineralization, where CO_2 is mineralized in subsurface geological formations, ex situ mineralization often utilizes readily accessible industrial by-products such as coal ash, iron and steel slags, mine wastes and tailings.[9–12] These by-products represent significant CO_2 storage potentials, with mine wastes and tailings alone estimated to have a potential to sequester 1.1-4.5 Gt CO_2 per year.[13] Furthermore, they tend to exhibit high reactivity, because these mineral by-products often contain finely ground particles and, in some cases, also a high amorphous content (e.g., high-temperature processed by-products such as coal ash and slag),[14–17] which could facilitate CO_2 storage at reduced costs. As such, ex situ mineralization has been widely investigated.[18,19]

Aqueous carbonation, i.e., carbonating minerals in an aqueous media containing dissolved carbonate species, is a commonly used method for ex situ mineralization.[20] It is generally believed that aqueous carbonation proceeds through interfacial coupled dissolution-precipitation (ICDP) reactions.[21,22] The process involves the dissolution of minerals (eq. 1):

$$2H^+ + H_2O + (Ca/Mg/Fe)SiO_3 \rightleftharpoons Ca^{2+}/Mg^{2+}/Fe^{2+} + H_4SiO_4 \quad (1)$$

Released cations ($Ca^{2+}/Mg^{2+}/Fe^{2+}$) further react with carbonate species in the solution, leading to the precipitation of insoluble carbonate minerals, such as calcite and its polymorphs ($CaCO_3$), dolomite ($CaMg(CO_3)_2$), and/or magnesite ($MgCO_3$) (eq. 2):[23]

$$Ca^{2+}/Mg^{2+}/Fe^{2+} + CO_2 + H_2O \rightarrow (Ca/Mg/Fe)CO_3 + 2H^+ \quad (2)$$

Regarding the ICPD mechanism, the mineral carbonation kinetics and degree can be governed by both mineral dissolution (Eq. 1) and subsequent carbonate precipitation (Eq. 2) reactions. It can be seen from Eq. 1 that providing more H^+ during the dissolution step should facilitate cation leaching from the minerals. Therefore, a common method to accelerate aqueous carbonation is to acidify the solution, sometimes in combination with adjustments to other solution conditions such as temperature, salinity, and the presence of ligands.[24–26] However, acidic conditions are not conducive to carbonate precipitation, as suggested by Eq. 2 where H^+ is a product. As such, a costly pH swing step, usually achieved through the provision of base,[27] ion-exchange,[28] or pressure/temperature swing involving CO_2 or ammonia,[29,30] is needed. The need to accelerate mineral dissolution through acidification has also largely prohibited the direct use of dilute CO_2 sources in accelerated aqueous carbonation without a dedicated capture process as it is difficult to achieve fast CO_2 dissolution into acidic aqueous solutions.

Alternatively, it was shown recently that accelerated aqueous carbonation using Ca-rich mineral feedstocks can be achieved through an autocatalytic basification process.[31] This approach involves a two-step, indirect carbonation process:

$$CaSiO_3 + Na_2CO_3 + 2H_2O \rightarrow CaCO_3 + 2NaOH + SiO_2 \quad (3)$$

$$2NaOH + CO_2\,(g) \rightarrow Na_2CO_3 + H_2O \quad (4)$$

In the first step described by Eq.3, aqueous carbonation is achieved with a soluble carbonate salt (Na_2CO_3 in this case). The carbonation reaction results in the formation of NaOH, which basifies the solution. After the carbonation step, the basic solution can be used to capture CO_2 from a variety of sources, described by Eq. 4, during which Na_2CO_3 is regenerated and can be used again by the carbonation step. Combining the two steps, mineralization is achieved without large pH swing between acidic and basic conditions.

The acceleration in mineral carbonation by Eq. 3 is hypothesized to be resulted from basification. Unlikely the acidification approach where cations are leached out of the mineral,

it is hypothesized that basic solution convert mineral surfaces into Ca-rich intermediate products (CIP) that can be easily carbonated.[31] The carbonation of CIP further generates more OH^-, creating an autocatalytic basification process. However, the hypothesis around the carbonatable CIP, especially their formation in relationship to mineral dissolution under basic conditions, remains to be confirmed. Furthermore, the role of silica, which tends to precipitate at low pH but remain in the solution at high pH, is unclear. If a strong coupling exists between these secondary phases and carbonation, it might be possible to enhance carbonation by promoting or suppressing their formation.

Considering this, we selected amorphous calcium silicate (CS, a representative alkaline-earth silicate) to study the role of secondary phases in aqueous mineral carbonation. We chose amorphous calcium silicate in this study because amorphous aluminosilicates are the main reactive mineral phases in coal ash used in the previous demonstration of accelerated aqueous carbonation through basification. We note that crystalline phases as well as the presence of other common mineral components such as Al_2O_3 may significantly alter the dissolution and carbonation behaviors, and they therefore warrant separate investigations. In this study, we designed aqueous carbonation routes that incorporated acid and base pretreatments of CS to investigate the effect of secondary phases formed under different conditions on carbonation. We focused on aqueous carbonation under basic conditions, which has been under-explored in the literature, and in particular aimed to examine the hypothesis that CIP formed under basic conditions can serve as the precursor to carbonate formation. Overall, we believe fundamental insights into aqueous mineral carbonation mechanisms over broad pH conditions could have strong implications in improving the process efficiency and economics of CO_2 mineralization.

MATERIALS AND METHODS.

Materials: Amorphous calcium silicate (CAS Number: 1344-95-2, Sigma-Aldrich)

was used in this study. The chemistry and amorphous nature of the sample were confirmed using energy dispersive X-ray (EDX) and X-ray diffraction (XRD, Figure S1A). The surface area of CS powders was determined to be 12.735 m^2/g by the Brunauer–Emmett–Teller (BET) method (Figure S1B). Reagent grade sodium carbonates (anhydrous) were purchased from Fisher Science. Colloidal silica was prepared by dispersing nanosilica powder (Sigma-Aldrich) in Na_2CO_3 solutions (Figure S2). Sodium silicate in liquid form was purchased from Sigma-Aldrich. The Si concentration was confirmed by Inductively Coupled Plasma Optical Emission spectroscopy (ICP-OES, CCD Simultaneous ICP-OES, VISTA-MPX, Varian, USA).

Batch carbonation with acid or base pretreatment: In this study, three carbonation routes with different pretreatments were applied to amorphous CS under ambient conditions (~25 °C, Figure 1A). The routes were designed as follows. Route I (Figure 1B) utilized CS pretreated with HCl solutions with different concentrations (10-100 mM) for three days. H^+ has been reported as a key factor for leaching Ca^{2+} from CS (eq.1).[32] However, leached H_4SiO_4 from CS can easily nucleate from solutions due to the low solubility (~2 mM) of SiO_2 phases under acid conditions, which might subsequently affect carbonations.[33,34] To suppress H_4SiO_4 nucleation, Route II uses NaOH (0-500 mM) to pretreat CS (Figure 1C). Because silica has a high solubility under basic conditions,[35] the precipitation of hydrated silica is suppressed although silica might precipitate in the form of CIP. In both routes, a liquid-to-solid ratio of 10 mL/g was used, and reactions took place in 15 mL polypropylene (PP) testing tubes. The tubes were vibrated using a vortex mixer during the experiments to agitate the slurry.

A high concentration of SiO_3^{2-} accumulating in the solution could have negative effects on carbonations since they can compete with aqueous carbonate species and decrease the activity of Ca^{2+} ions (Table S1).[36] Therefore, another route with NaOH (0-500 mM) pretreatment, Route III (Figure 1D), was designed as follows: after the same NaOH pretreatment as Route II, the liquid phase was removed by a pipette after 5 min centrifugation at 9000 g, and the remaining solid phase were used for further carbonation. The removed CS accounted for less than 10 wt. % of the original CS.

Following the pretreatment in each route, slurry carbonation experiment was conducted directly in the PP testing tube under the ambient condition (~25 °C). A Na_2CO_3 stock solution was added into the testing tube to reach a liquid to solid ratio of 20 mL/g and 1 M Na_2CO_3 in the carbonation solution for all batch experiments. The tubes were vibrated using the vortex mixer during carbonation as well.

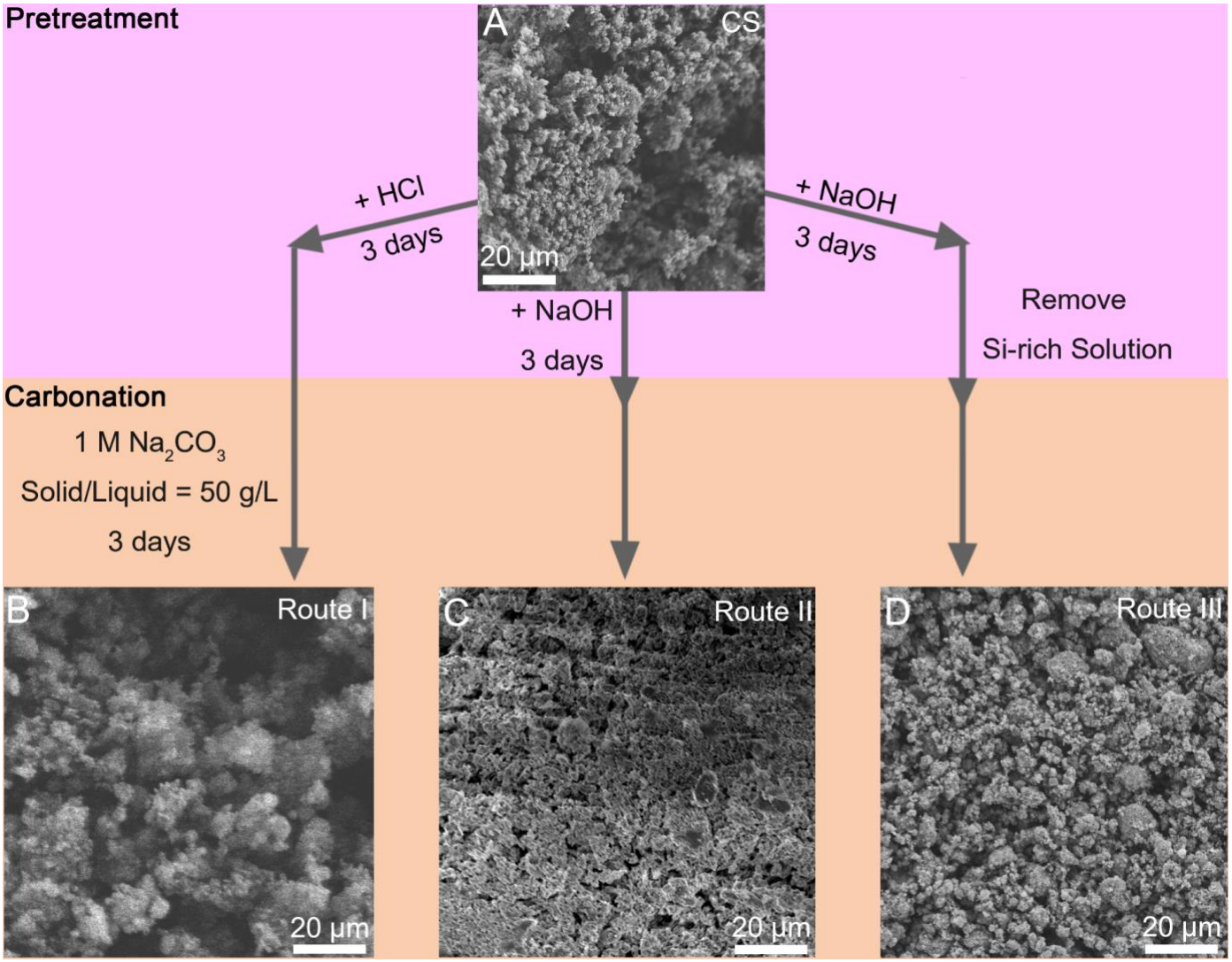

Figure 1. The three carbonation routes investigated in this study with example SEM images of the raw and carbonated calcium silicate (CS). SEM images of (A) initial CS, carbonated CS via Routes (B) I, (C) II, and (D) III.

Collecting carbonated samples: After three days of carbonation, the solid and liquid phases were separated using a centrifuge (Allegra 25R Centrifuge, Beckman Coulter, USA) at 9000 g for 5 min. Collected solids were washed three times with DI water to remove residual

190 salt solutions and then dried in an oven (Isotemp Oven Model 655F, Fisher Scientific) at 100 ℃
191 for 24 h. This washing procedure was effective for removal of residual Na_2CO_3, which was
192 confirmed by EDX (Figure S4) spectrum and thermogravimetric analysis (TGA, Figure S5).

193 **Carbonation degree quantifications:** The carbonation degree was defined as the
194 percentage of carbonated calcium with respect to the total calcium content. To quantify
195 carbonation degrees, the TGA (TA 5500, USA) and ICP-OES results were combined. The TGA
196 was performed using ~15 mg of washed sample under a N_2 condition with a gas injection rate
197 of 100 mL/min and a heating rate of 10 K/min from 30 ℃ to 950 ℃. For all samples, TGA
198 curves contained three distinct regions: (1) evaporable water loss (30-200 ℃), (2) bound water
199 loss (200-550 ℃), and (3) CO_2 release (i.e., calcium carbonate decomposition; 550-800 ℃).
200 The CO_2 content (w_{CO_2}) was determined from TGA curves using the weight loss from 550 to
201 800 ℃. To measure total CaO content (C_{CaO}) within the carbonated samples, dried powders (<
202 0.5 mg) were dissolved in 5 M HNO_3 and then diluted up to 10 times for ICP-OES
203 measurements. The CaO-conversion into $CaCO_3$ (η_{Ca}; or carbonation degree) was calculated
204 with eq.3.

205 $$\eta_{Ca} = \frac{w_{CO_2} \times M_{CaO}}{M_{CO_2} \times C_{CaO}} \quad (3)$$

206 in which M_{CaO} and M_{CO_2} are molecular weights of CaO (56.08 g/mol) and CO_2 (44.01 g/mol).
207 All data presented in this study were derived from three independent experiments.

208 **Solid sample characterizations:** A scanning electron microscopy (SEM, LEO 1530,
209 Zeiss, Germany) equipped with EDX was used to observe the morphologies and determine the
210 elemental compositions of carbonated samples. Dry powders were mounted onto aluminum
211 (Al)-SEM stub stands using copper (Cu)-tapes and coated with gold (~8 nm, Prep-Leica
212 ACE600 Deposition, Leica, Germany) to increase the electrical conductivity. SEM images were
213 taken with an acceleration voltage of 5 kV and collected using the secondary electron detector.
214 For elemental analyses, EDX was performed with an acceleration voltage of 10 kV, and the

signal from the sample was recorded using the Quasor II EBSD System (ThermoFisher Scientific, USA). To detect the crystallinity of newly formed $CaCO_3$ phases, carbonated samples were characterized using x-ray diffraction (XRD, D8 Discovery, Bruker, Germany) with incident Cu *Kα* radiation (λ = 1.54178 Å). The data acquisition was achieved at four scanning steps from 20° to 60° with a rate of 120 s/step.

For nanoscale characterization, high resolution transmit electron microscopy (HRTEM) was performed to directly observe crystallographic phases within the particles.[37] HRTEM samples were prepared by dropping 10 μL suspension samples on to a copper grid (G200-CU: Electron Microscopy Sciences gilder standard square 200 mesh copper grid) after carbonation experiments. The residual solution was removed by placing a piece of filter paper at the edge of the grid. Deposited particles were washed three times by dropping 10 μL DI water. HRTEM images were collected using TF30 (FEI Tecnai TF30 TEM, Thermo Fisher Scientific, USA) with an acceleration voltage of 300 kV. Before collecting each image, we performed focusing on a nearby area to prevent beam damages. Measured *d*-spacing values were used to identify crystalline species. The standard parameters for calcite (# 47-1743), aragonite (# 41−1475), wollastonite (# 42−0550), and Na_2CO_3 (# 25−0815) were found in JCPDF and used as references (Figure S6).

Acid and base pretreated samples were lyophilized (freeze-dried) and characterized using TGA and X-ray photoelectron spectroscopy (XPS). XPS, for surface analyses, was executed under an ultra-high vacuum condition (5×10^{-10} Torr) using a Thermo K alpha X-ray Photoelectron Spectrometer (Thermo Scientific, USA) equipped with a monochromatic Al Ka X-ray source (hν = 1486.6 eV) at 75 W with a detection pass energy of 20-80 eV. All binding energies were calibrated to the common C 1s peak at 284.6 eV. Thermal Advantage software (Thermo Scientific, USA) was used to analyze the collected XPS data with smart background methods for baseline correction and Gaussian function for peak fittings.[38]

Solution analyses: After the carbonation procedures, the separated solutions were

passed through syringe filters (220 nm, Millex-GP, Millipore Express) to remove residual particles. Then, obtained solutions were acidified and diluted up to 10 times using 0.5 M HNO_3 for dissolved elemental analyses using ICP-OES. All concentrations were reported as the averages of three independent measurements.

***In situ* observations of carbonation:** Raman Spectrometer (LabRAM HR Evolution, Horiba, France) was used to monitor aqueous carbonate species *in situ*. The spectra were collected with a laser at 532 nm followed a calibration by the characteristic band of silicon at 520.7 cm^{-1}.[39] The spectra of Na_2CO_3 (pH 12, adjusted by 1 M NaOH) solutions with and without SiO_2 (including colloidal silica and Na_2SiO_3) were collected every 24 h up to 72 h with a 10× objective lens. To quantify the CO_3^{2-}, 100 mM $NaNO_3$ was added as a reference since its concentration did not change during carbonation (Figure S7). The in situ Raman characterizations were used to study the effects of solution silica (colloidal silica and Na_2SiO_3) on CS carbonation in basic solutions. Collected Raman data were analyzed using the LabSpec 6 software (LabRAM HR Evolution, Horiba, France).

PHREEQC simulations: PHREEQC Interactive Version 3.3.7.11094 was used to simulate carbonating reaction based on solution chemistry determined by ICP-OES with the wateq4f database.[40] The solubility products of several CIP not included in the database were obtained from the literature (Table S2). The simulations were performed through two steps: in the first step, the initial solution was equilibrated to calculate the activities of each solute (including Ca^{2+}, CO_3^{2-}, and H_4SiO_4. In the second step, the solution was allowed to equilibrate to calculate the saturation indices (SI) with respect to possible CS/CIP/SiO_2/$Ca(OH)_2$/$CaCO_3$ phases. The relative supersaturation of precipitating phases can be expressed by[41]

$$\sigma = \log IAP - \log K_{sp} \quad (4)$$

where σ is the saturation index (σ > 0 means thermodynamically favorable for nucleation), IAP is the actual ion activity products, and K_{sp} is their corresponding values at equilibrium. For instance, the σ of $Ca(OH)_2$ can be expressed by

$$\sigma = \log \{[a(Ca^{2+})][a(OH^-)]^2\} - \log K_{sp} \quad (5)$$

where $a(Ca^{2+})$ and $a(OH^-)$ are the activities of Ca^{2+} and OH^- ions.

RESULTS AND DISCUSSIONS

CS dissolution behaviors during pretreatments.

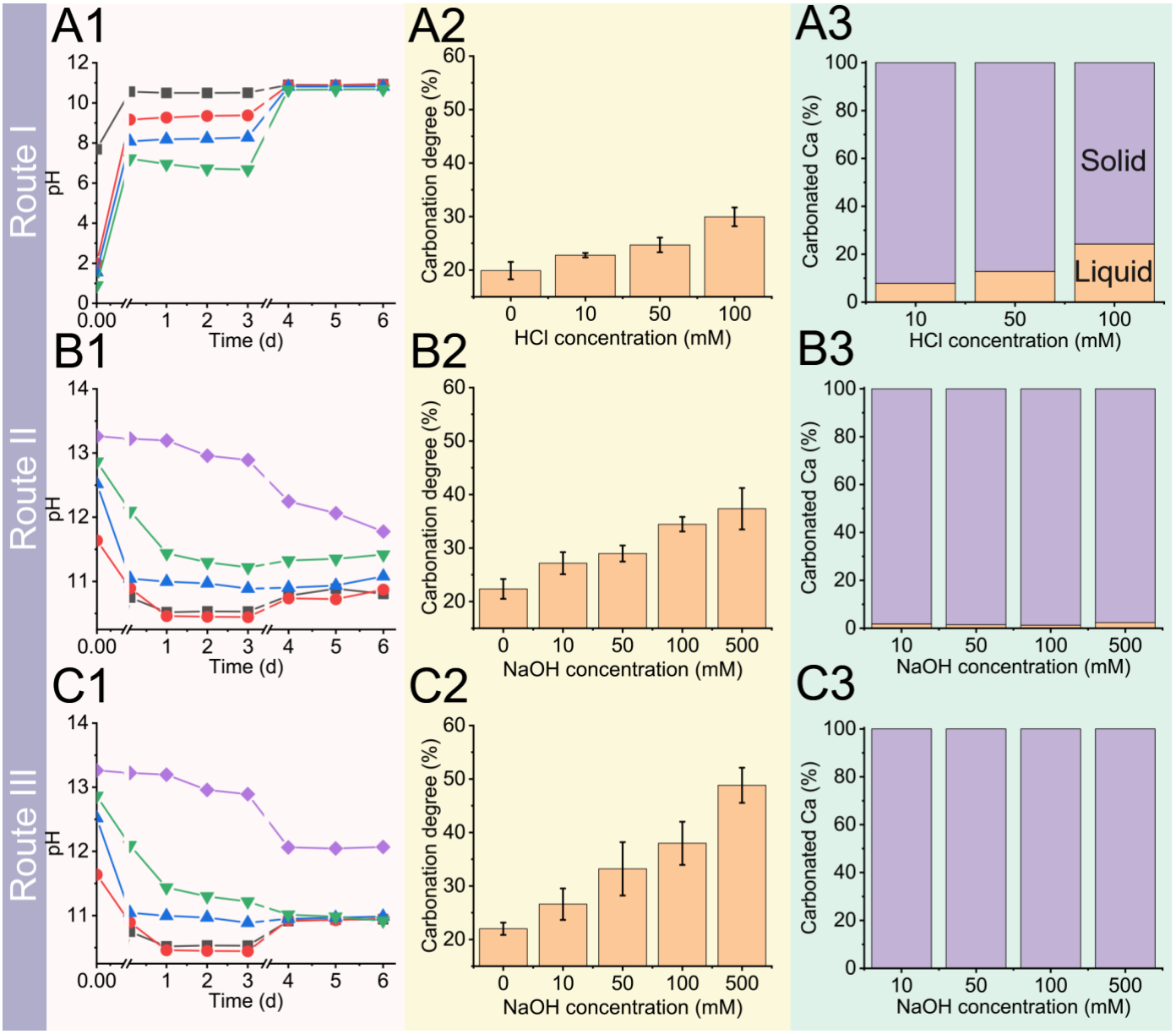

Figure 2. Quantifications of CS carbonations via Routes I, II, and III. (A1), (B1), and (C1) respectively show the pH evolution during the pretreatment step of the three routes. (A2), (B2), and (C2) show the carbonation degree calculated based on eq.3. (A3), (B3), and (C3) show the source of the carbonated Ca, i.e., leached Ca precipitated from the liquid (orange) vs. solid bound Ca (purple).

During the pretreatment, pH approached a steady state in all cases within 3 days (Figure

2A1, B1, and C1). In Route I, an initial rapid increase in pH was observed due to the consumption of H^+ (Figure 2A1). The final pH and [Ca^{2+}] in the solution, after three days, ranged from 7 to 11 and 4.87 to 64.69 mM, respectively (Figure 3A). Even though 500 mM HCl released more Ca^{2+} into solutions, the final pH was at ~1.0 after pretreatment (Figure S8A). As this study focuses on carbonation under basic conditions, we limited the HCl concentration ranging from 0 to 100 mM. In contrast with the rapid release of Ca^{2+}, the Si concentrations in the liquid phases remained constant and their values (~5 mM) were above saturated levels of SiO_2 species (> 2 mM, Figure 3A). In Route II, the dissolution of silica led to the consumption of OH^- and a decrease in pH (Figures 2B1 and C1). After three days of reactions, the concentrations of soluble SiO_2 reached 13.65 to 66.64 mM (Figure 3B). [Ca^{2+}] in the solution was very low, which is expected since CIP have very low solubilities at high pH.

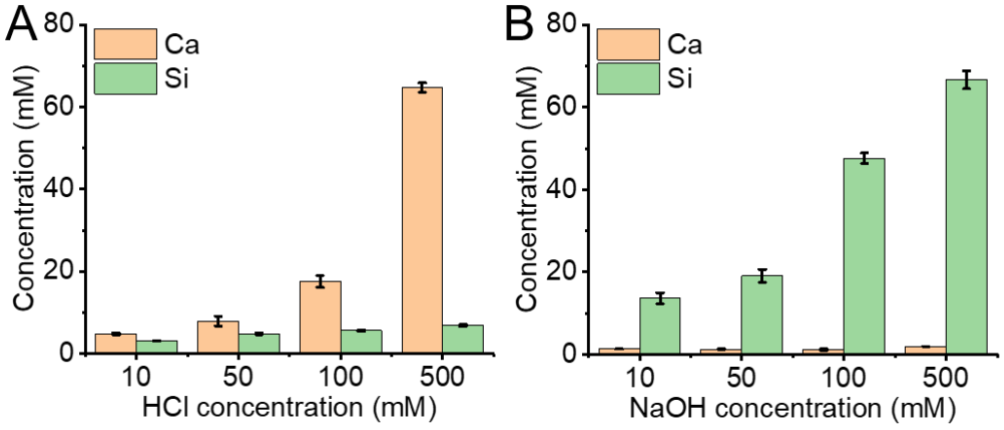

Figure 3. The distribution of elements in solutions after (A) HCl and (B) NaOH pretreatments. With a higher concentration of HCl, more Ca^{2+} was leached from the samples. Conversely, NaOH pretreatments resulted in a higher release of Si into the solutions.

Carbonation of CS after pretreatments. After the pretreatment, carbonation experiments were performed, and the carbonation degrees were quantified, as explained in the method section. Results of the TGA and ICP-OES analyses are included in the Supporting Information (Figure S9 and S10). As shown in Figures 2A2, B2, and C2, increasing [HCl] (from 0 to 100 mM) in Route I or [NaOH] (from 0 to 500 mM) in Route II and III resulted in higher carbonation degrees, suggesting that enhancing dissolution through the pretreatments facilitates carbonation. In Route I, 100 mM HCl presented the highest carbonation degree of 28%.

Interestingly, the amount of converted Ca (0.57-0.73 mmol) far exceeded the Ca^{2+} (0.05-0.18 mmol) released into the solution by the HCl pretreatment. This suggested that most of carbonated Ca^{2+} came directly from the remaining solids—these solid-bound Ca^{2+} ions accounted for 75-91% of the total carbonation degree following the HCl pretreatment (Figure 2A3). However, the absolute amount of carbonated solid-bound Ca^{2+} remained roughly constant at ~0.54 mmol for all HCl pretreated cases, regardless of [HCl] or dissolved [Ca^{2+}].

Comparing to the HCl pretreatment, the NaOH pretreatments (Routes II and III) led to higher carbonation degrees. In these two routes, nearly all carbonated Ca^{2+} came from the residual solids (Figures 2B3 and C3). Between the two NaOH pretreatment routes, Route III, in which the liquid phase was removed after the pretreatment, had a higher carbonation degree, especially at higher NaOH concentrations (Figures 2B2 and C2). The highest carbonation degree of 49%, among all cases in this study, was achieved with 500 mM NaOH through Route III (Figure 2C2). This suggested that reducing solubilized SiO_2 can further increase carbonation efficiencies under basic conditions.

Characterizations of carbonated CS samples. The carbonated CS samples were characterized to assess their chemistry, morphology, and mineralogy. Based on EDX analyses, carbonated samples exhibited similar chemistry as uncarbonated CS except for enhanced carbon content (Figure S4). The XRD spectra confirmed the presence of calcium carbonate polymorphs including calcite and aragonite (Figures 4A, D, and G). Additionally, HRTEM analyses identified crystalline particles (area 1) within an amorphous matrix (area 2) (Figures 4B, E, and H). The measured *d*-spacing (3.03 Å) of lattice planes of these crystallized phases indicated that their most likely phase is calcite ($d_{(104)}$ = 3.0355 Å, JCPDF 47-1743). In contrast to the Route I sample (100 mM HCl pretreatment) less crystallized phases were detected (Figure 4B), more calcites were found at particle surfaces in samples from Routes II (100 mM NaOH, Figure 4E) and III (100 mM NaOH, Figure 4H). The HRTEM confirmed that, in addition to coarse, discrete calcium carbonate particles (Figure S11), the carbonation products can be

present in the form of nanocrystals enclosed in an amorphous matrix that most likely consists of silica. According to PHREEQC simulations (Tables S3 and S4), silica was undersaturated during carbonation in all three routes, which means the condensation of silica from the solution should not occur simultaneously with the carbonate precipitation. The presence of carbonate nanocrystals within the amorphous matrix suggested that the surface of pretreated CS did not fully inhibit carbonation. This agrees with previous observations.[42] However, such a layer is expected to slow the diffusion of aqueous species if it is formed on the CS surface since the carbonation kinetics is somewhat diffusion limited, as suggested by the reduced carbonation degree under the stagnant condition comparing to the agitated condition (Figure S3A and S3B). The other explanation is the direct conversion of CS/CIP to carbonates, in which CS/CIP was decalcified into the silica matrix surrounding the carbonate nanocrystals.[43] It should be noted that, even though the solution is undersaturated, the dissolution of the silica is kinetics-limited and therefore significant portions of the silica matrix formed this way can still remained in the solid residue.

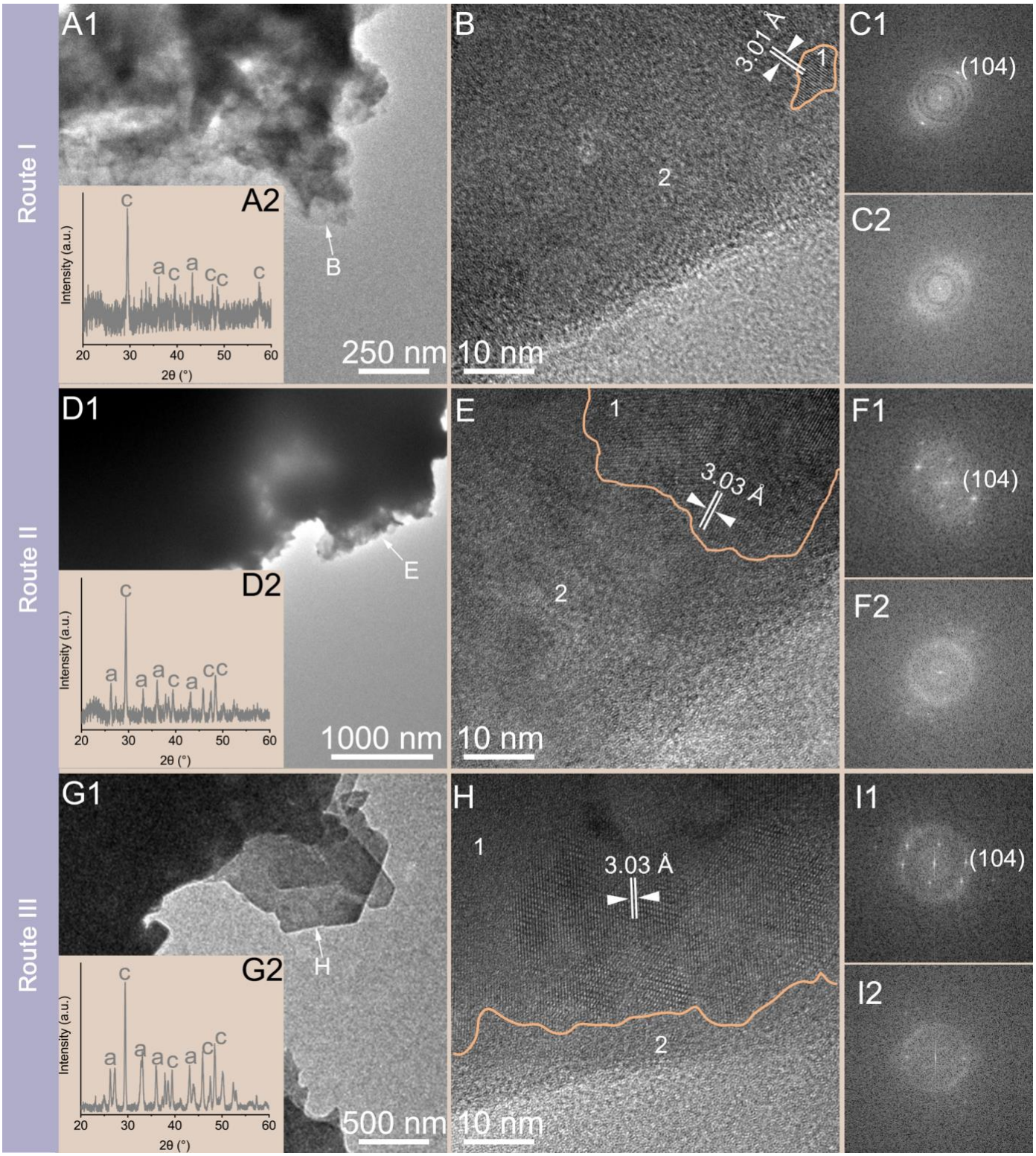

Figure 4. Identifications of the precipitates in CS carbonated via (A-C) Route I (100 mM HCl), (D-F) Route II (100 mM NaOH), and (G-I) Route III (100 mM NaOH). (A2, D2, and G2) show XRD spectra confirming the presence of calcite (c, Figure S6A) and aragonite (a, Figure S6B) within the carbonated CS. (A1, D1, and G1) Low magnification TEM and corresponding HRTEM images (B, E, and H) of selected areas marked by arrows show the distributions of calcite within the amorphous phase. The crystalline (marked by 1) and amorphous (marked by 2) phases are separated by orange lines. Corresponding FFT patterns collected from area 1 and 2 were gave in C, F, and I respectively.

Characterizations of intermediate products from the pretreatments. Results so far have suggested that the carbonation degree followed the order of Route III > Route II > Route I. Most notably, the increase in carbonation degree from the NaOH pretreatment (Routes II and III) comparing to the HCl pretreatment (Route I) is significant. To understand the different alterations of the CS samples through acid and base pretreatments, pretreated CS powders were lyophilized and subsequently characterized using TGA and XPS. For both acid and base treated samples, TGA only showed a small and simple weight loss (< 10%) up to 200 ℃, which can be attributed to water loss. No distinct dehydration behaviors associated with crystalline phases (e.g., weight loss at 385 ℃ for $Ca(OH)_2$)[44] were observed in the NaOH treated samples (Figures 5A1 and A2). We complemented these results with PHREEQC simulations (Tables S3 and S4). Based on the solution chemistries from ICP-OES, our simulations indicated that only amorphous SiO_2 is supersaturated at end of the 100 mM HCl-pretreatment, suggesting that SiO_2 precipitation is possible (Table S3). When it comes to the NaOH pretreatment, the solutions were supersaturated with respect to various CIP products (Ca/Si 1.20~1.59).

We further performed XPS analyses to investigate the surface elemental compositions (depth range of 0-10 nm) of HCl/NaOH-treated CS samples. We used peak intensities at 348 and 103 eV, which correspond to Ca $2p^{2/3}$, and Si 2p respectively, to evaluate whether surface is enriched with Ca or Si (Figure 5D). For raw CS, the intensity ratio of Ca $2p^{2/3}$ to Si 2p, I(Ca)/I(Si), was ~0.24, while the ratios of HCl (100 mM)-treated and NaOH (100 mM)-treated CS were found to be ~0.2 (slightly Si-enriched) and ~2.1 (significantly Ca-enriched), respectively (Figure 5D). Higher NaOH concentrations led to further surface enrichment of Ca with I(Ca)/I(Si) of ~2.6 observed at 500 mM. For the HCl-pretreatment, the enrichment of Si is reasonable since amorphous SiO_2 was supersaturated and the solution had high [Ca^{2+}]. For the NaOH-pretreatments, the formation of Ca-rich surfaces should be due to the precipitations of CIP. It should be noted, however, compositions of the precipitated CIP may deviate from the equilibrium phases suggested by the PHREEQC simulations (Table S4). It is interesting that TGA data did not show substantial formation of hydrates in the NaOH pretreated samples

(Figures 5A-C). In particular, the 500 mM NaOH pretreatment resulted in lower amounts of bound water than 100 mM NaOH, even though it exhibited higher Ca enrichment (i.e., more CIP precipitation). This could be due to the formation of non-equilibrium phases or a shift to high Ca/Si ratio hydration products. The nature of those intermediate products warrants further investigation as they could play a critical role in aqueous mineral carbonation.

The surface modifications of CS through acid and base pretreatments had direct impact on the carbonation degree. Most studies so far have focused on Si-rich layers formed under acidic conditions. According to recent studies, such Si-rich layers formed at the particle surfaces have limited effects on aqueous carbonation.[42,45–47] Schott *et al*. (2012) found that, for CS, the newly formed amorphous SiO_2 layer did not create a diffusion barrier for aqueous species such carbonate ions.[48] Similar results were reported by Yujia *et al*. (2017 and 2018).[42,45] Our observations in Route I are consistent with those studies. Although increasing HCl concentration led to more Ca leaching out and therefore more SiO_2 precipitation (e.g., the Si-enriched surface observed by XPS), the pretreatment did not significantly affect the amounts of Ca carbonated directly from the treated solids (solid-bound Ca), as discussed in the earlier section. One explanation is that the Si-rich layer did not form directly on the mineral surface, a phenomenon that has been observed during silicate glass dissolution.[49,50]

In contrast, under basic conditions, CIP with a high Ca/Si ratio can form via coupled dissolution and precipitation processes. The correlation between surface Ca enrichment and carbonation degree observed in NaOH pretreated CS suggest that those CIP products serve as precursors to carbonation. The decalcification of loosely packed CIP products due to carbonation and subsequent condensation of the remaining silica network around the nucleated calcium carbonate can explain the structures observed commonly in Route II and III samples by HRTEM, i.e., formation of nanocrystals enclosed in the amorphous silica matrix. The implication is that base pretreatment may be able to transform minerals like CS into intermediate phases that can be readily carbonated. In another word, base pretreatment or carbonation under basic conditions could offer an effective route for aqueous mineral

carbonation.

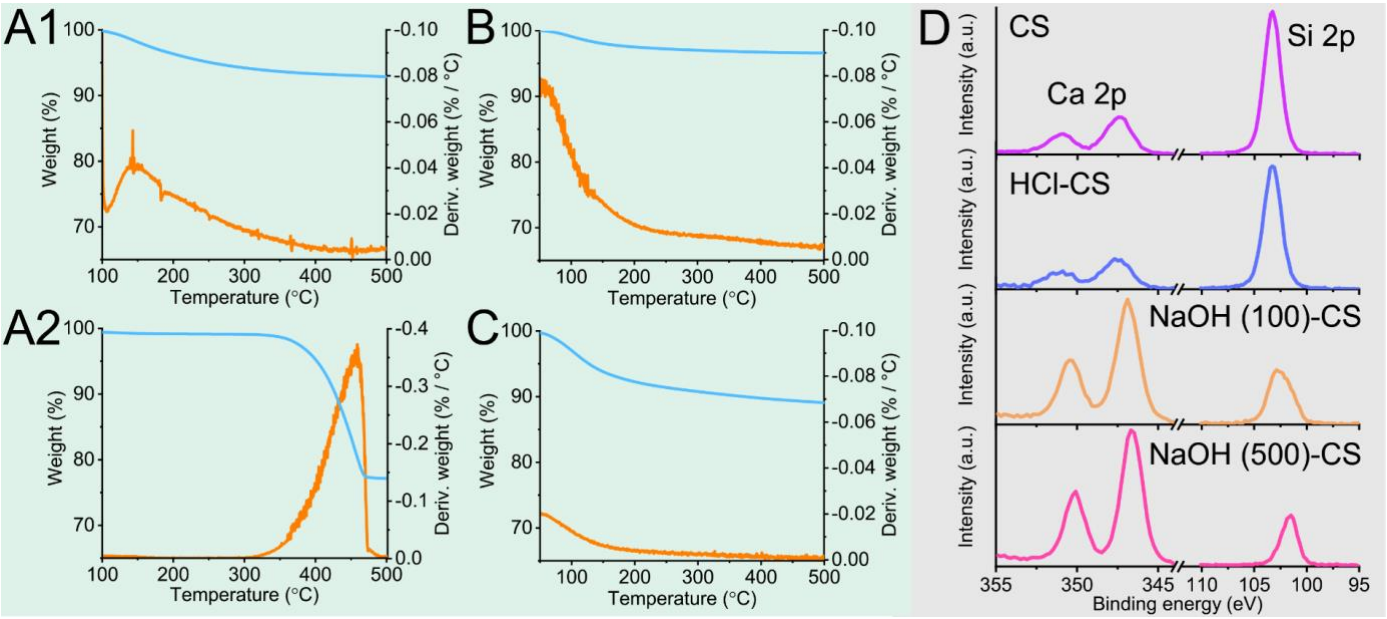

Figure 5. Characterizations of pretreated CS. TGA data are shown for (A1) HCl-pretreated CS, (A2) $Ca(OH)_2$, (B) 100 mM NaOH pretreated CS, and (C) 500 mM NaOH pretreated CS. Blue and orange curves are weight-temperature and corresponding derivative weight curves, respectively. (D1) shows XPS collected from pretreated CS samples.

Effects of aqueous silica/silicate on $CaCO_3$ formation. For carbonation under basic conditions (Route II and Route III), the carbonation degree could be affected by the presence of aqueous Si species. This can be seen when comparing Route II (the carbonating solution contained dissolved Si) with Route III (the fresh carbonating solution did not contain dissolved Si). To understand this phenomenon, we applied Raman spectroscopy to monitor the carbonation kinetics in the presence of aqueous Si *in situ*. We prepared 1 M Na_2CO_3 solutions containing 0-200 mM [Si] in two forms—colloidal SiO_2 or solubilized Na_2SiO_3—at pH 12 and subsequently used them to carbonate raw CS (Figures S12A and B). We used the peak at ~1066 cm^{-1}, corresponding to the characteristic symmetric C−O stretching mode, to monitor the carbonate group in the solution ($CO_3^{2-}{}_{aq}$; Figure S12C1).[51] When CO_3^{2-} precipitate into $CaCO_3$, the peak would shift to ~1085 cm^{-1} and this was utilized to track the carbonation kinetics (Figure S12C2).[52] Furthermore, we added 100 mM $NaNO_3$ in the solution as a reference (~1049 cm^{-1} for NO_3^-, Figures S12D1, D2, and D3).[53] NO_3 would remain in the solution during the

carbonation experiment, thereby allowing us to track carbonate precipitation through the intensity ratio of $CO_3^{2-}{}_{aq}$ to NO_3^-, $I(CO_3^{2-}{}_{aq})/I(NO_3^-)$. As can be seen in Figures 6A and B, $I(CO_3^{2-}{}_{aq})/I(NO_3^-)$ decreased with time during the carbonation processes, indicating the precipitation of aqueous carbonate groups. We compare precipitation kinetics by calculating the CO_3^{2-} consumption rate, R, based on the decrease in $I(CO_3^{2-}{}_{aq})/I(NO_3^-)$ over the experiment period, $\Delta[I(CO_3^{2-})/I(NO_3^-)]$:

$$R = \frac{\Delta[I(CO_3^{2-})/I(NO_3^-)]}{t}$$

where t=3 days. Adding extra colloidal SiO_2 and Na_2SiO_3 solutions decelerated the carbonation kinetics, and a higher Si concentration showed a stronger effect in suppressing the carbonation kinetics (Figures 6A and B). Compared with colloidal SiO_2, the inhibition effect of solubilized SiO_3^{2-} was much greater (Figure 6C). This confirms that removing Si-rich solutions in Route III should indeed help improve the carbonation degree.

The suppressing effect of aqueous SiO_2 on mineral carbonation can occur through various mechanisms. Dissolved SiO_2 could suppress the dissolution of solid-bound Si species.[50] This constrains the kinetics through coupled dissolution and precipitation pathway, leading to a lower degree of carbonation. Dissolved Si can also regulate and slow down $CaCO_3$ nucleation, limiting the precipitation kinetics. This effect has been well recognized by previous studies.[41,54] According to classical nucleation theory, the inhibition of $CaCO_3$ nucleation in the presence of soluble Si has a close relation with the Ca^{2+} activity. At pH 12, aqueous silica species and the surfaces of SiO_2 colloids are negatively charged (Figure S2),[55] which leads to the sequestration of dissolved Ca^{2+} ions and subsequently a decrease in the Ca^{2+} activity by forming [SiO_2-Ca^{2+}] complexes (may involve multi-nuclear, kinetically-inert surface complexes).[26] Therefore, the presence of aqueous SiO_2 has an inhibition effect on $CaCO_3$ nucleation. A similar inhibition effect was also reported in previous studies with the addition of other anions, such as SO_4^{2-}.[56,57]

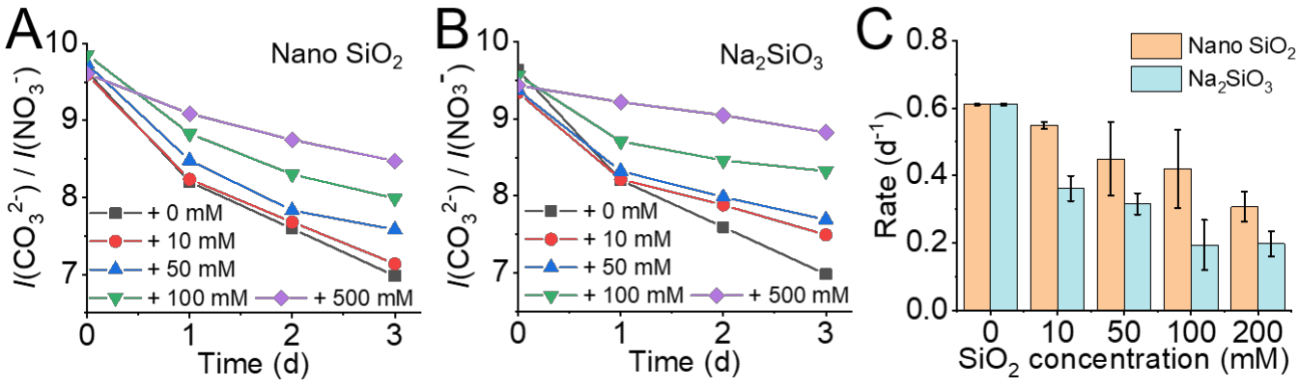

Figure 6. *In situ* observation of $CaCO_3$ nucleation in the absence and presence of (A) silica colloids (nano SiO_2) or (B) solubilized silicates (Na_2SiO_3) using a Raman microscope. (C) summarizes the corresponding CO_3^{2-} consumption rates (R)

ENVIRONMENTAL IMPLICATION. Ex situ mineralization is an effective and scalable pathway to remove CO_2, the main driver of global warming, from the atmosphere.[58] In this study, we demonstrated three aqueous mineral carbonation routes using amorphous CS as an example mineral feedstock. All three routes were based on carbonation in basic conditions but involved pretreatments of CS under different solution conditions (Figure 1). As shown by the results, acid and base pretreatments both promoted the dissolution of CS and enhanced the carbonation degree (Figure 2). Under acidic conditions, the solution became easily supersaturated with amorphous silica (~ 2 mM), and a Si-rich layer formed on the mineral surface. In agreement with previous observations,[42] the newly-forming silica layers did not show strong effects on carbonation. Thus, the main effect of the HCl pretreatment was to leach Ca into the solution, e.g., forming circumneutral $CaCl_2$ solution if no other types of dissolution occur. Converting leached Ca into carbonate precipitate would consume roughly stoichiometric amount of base or require a high CO_2 pressure to substantially shift equilibrium. As such, traditional carbon mineralization approaches utilizing acid leaching require either a large pH swing or high-pressure CO_2. The cost, energy consumption, and CO_2 footprint for generating base and/or obtaining concentrated/pressurized CO_2 have been one of the main challenges for carbon mineralization.

Alternatively, CS can be pretreated by bases, the effect of which has been relatively

less studied. Here, we demonstrated that, for amorphous CS, pretreatment with more concentrated base (at least up to 500 mM) resulted in higher carbonation degree. Based on material characterization, we attributed this effect to the formation of readily carbonatable CIP, which is in agreement with the hypothesized mechanism for aqueous carbonation under basic conditions.[31] Utilizing this mechanism to achieve accelerated mineral carbonation provides a critical benefit—because dissolution enhancement and carbonate precipitation are now both performed under basic conditions, large pH swing can be avoided. Furthermore, through the regeneration of Na_2CO_3 via Eq. 4, accelerated aqueous carbonation under basic conditions can be used to directly couple mineralization with carbon capture, subsequentially reducing the overall energy demand and cost for carbon removal. The effectiveness and techno-economic benefits of such an approach have been recently demonstrated for direct air capture and sequestration of CO_2 using coal fly ashes (complex mixtures of Ca-rich aluminum silicates).[31] Here, we showed that the key to this approach lies in the control of aqueous Si species including solubilized silicate and colloidal silica, which may be manipulated utilizing the complex behavior of silica dissolution and condensation in response to pH, ionic species, and ionic strength. Identifying optimal reaction conditions or process designs to mitigate the inhibitive effect of aqueous Si species on mineral dissolution and carbonate precipitation could enable low-cost and highly efficient ex situ mineralization-based carbon removal methods.

So far, studies on aqueous carbonation involving strongly basic conditions have been very limited. This study has used amorphous CS as an example system. The carbonation behavior of more realistic mineral feedstocks requires further studies. Crystalline minerals and the effect of other common oxide components such as magnesia and alumina in particular warrant detailed investigations. Furthermore, understandings on critical issues like the nature and formation mechanism/kinetics of CIP remain lacking. Overall, this study indicates that fundamental studies on aqueous mineral carbonation in a much broader range of pH and solution conditions are critically needed for the development of efficient aqueous mineral carbonation methods.

ASSOCIATED CONTENT

Supporting Information. The Supporting Information is available free of charge on the ACS Publications website.

Reaction constants of calcium silicate complexes (Table S1); equilibrium constants for calcium silicate hydrates (Table S2); PHREEQC simulations (Table S3 and S4); characterization of calcium silicate (Figure S1); characterizations of Si-species (Figure S2); mixing system (Figure S3); energy dispersive X-ray spectra (Figure S4); thermogravimetric analyses (Figure S5); X-ray diffractions of standards (Figure S6); $NaNO_3$ concentrations within carbonating solutions (Figure S7); pH, [Ca], and [Si] within solutions during pretreatments (Figure S8); carbonation degree analyses (Figures S9 and S10); SEM images of carbonated CS and solution grown calcite crystals (Figure S11); characterizations of Si-species (Figure S12).

AUTHOR INFORMATION

Corresponding Authors

Hang Zhai − *Department of Civil and Environmental Engineering, University of Wisconsin-Madison, Madison, Wisconsin 53706, United States*; orcid.org/0000-0002-8161-448X; Email: hzhai25@wisc.edu

Bu Wang − *Department of Civil and Environmental Engineering, University of Wisconsin-Madison, Madison, Wisconsin 53706, United States*; orcid.org/0000-0002-9294-0918; Email: bu.wang@wisc.edu

Authors

Qiyuan Chen − *Department of Civil and Environmental Engineering, University of Wisconsin-Madison, Madison, Wisconsin 53706, United States*

Mehmet Yilmaz − *Department of Civil and Environmental Engineering, University of Wisconsin-Madison, Madison, Wisconsin 53706, United States*

Notes

The authors declare no competing financial interest.

ACKNOWLEDGEMENTS

We thank Jinhua Ji for his help with figure drawings. This material is based upon work supported by the National Science Foundation under Grant No. 2132022. The information, data, or work presented herein was funded in part by the Advanced Research Projects Agency-Energy (ARPA-E), U.S. Department of Energy, under Award Number DE-AR 0001636. The authors gratefully acknowledge use of facilities and instrumentation at the UW-Madison Wisconsin Centers for Nanoscale Technology (wcnt.wisc.edu) partially supported by the NSF through the University of Wisconsin Materials Research Science and Engineering Center (DMR-1720415).

REFERENCE.

(1) IPCC, 2022: Climate Change 2022: Mitigation of Climate Change. Contribution of Working Group III to the Sixth Assessment Report of the Intergovernmental Panel on Climate Change [P.R. Shukla, J. Skea, R. Slade, A. Al Khourdajie, R. van Diemen, D. McCollum, M. Pathak, S. Some, P. Vyas, R. Fradera, M. Belkacemi, A. Hasija, G. Lisboa, S. Luz, J. Malley, (eds.)]. Cambridge University Press, Cambridge, UK and New York, NY, USA. doi: 10.1017/9781009157926.

(2) Rackley, S. Carbon Capture and Storage. *Carbon Capture and Storage* **2009**, *325* (September), 1–392. https://doi.org/10.1016/C2009-0-19306-6.

(3) Bui, M.; Adjiman, C. S.; Bardow, A.; Anthony, E. J.; Boston, A.; Brown, S.; Fennell, P. S.; Fuss, S.; Galindo, A.; Hackett, L. A.; Hallett, J. P.; Herzog, H. J.; Jackson, G.; Kemper, J.; Krevor, S.; Maitland, G. C.; Matuszewski, M.; Metcalfe, I. S.; Petit, C.; Puxty, G.; Reimer, J.; Reiner, D. M.; Rubin, E. S.; Scott, S. A.; Shah, N.; Smit, B.; Trusler, J. P. M.; Webley, P.; Wilcox, J.; Mac Dowell, N. Carbon Capture and Storage (CCS): The Way Forward. *Energy Environ. Sci.* **2018**, *11* (5), 1062–1176. https://doi.org/10.1039/c7ee02342a.

(4) Ma, J.; Li, L.; Wang, H.; Du, Y.; Ma, J.; Zhang, X.; Wang, Z. Carbon Capture and Storage: History and the Road Ahead. *Engineering* **2022**, *14*, 33–43. https://doi.org/10.1016/j.eng.2021.11.024.

(5) Daval, D.; Martinez, I.; Guigner, J. M.; Hellmann, R.; Corvisier, J.; Findling, N.; Dominici, C.; Goffé, B.; Guyot, F. Mechanism of Wollastonite Carbonation Deduced from Micro- To Nanometer Length Scale Observations. *Am. Mineral.* **2009**, *94* (11–12), 1707–1726. https://doi.org/10.2138/am.2009.3294.

(6) Todd Schaef, H.; McGrail, B. P.; Loring, J. L.; Bowden, M. E.; Arey, B. W.; Rosso, K. M. Forsterite [Mg2SiO4)] Carbonation in Wet Supercritical CO2: An in Situ High-

555 Pressure X-Ray Diffraction Study. *Environ. Sci. Technol.* **2013**, *47* (1), 174–181.
556 https://doi.org/10.1021/es301126f.

557 (7) Qafoku, O.; Kovarik, L.; Kukkadapu, R. K.; Ilton, E. S.; Arey, B. W.; Tucek, J.; Felmy,
558 A. R. Fayalite Dissolution and Siderite Formation in Water-Saturated Supercritical CO
559 2. *Chem. Geol.* **2012**, *332–333*, 124–135.
560 https://doi.org/10.1016/j.chemgeo.2012.09.028.

561 (8) Shao, H.; Ray, J. R.; Jun, Y. S. Dissolution and Precipitation of Clay Minerals under
562 Geologic CO 2 Sequestration Conditions: CO2brinephlogopite Interactions. *Environ.*
563 *Sci. Technol.* **2010**, *44* (15), 5999–6005. https://doi.org/10.1021/es1010169.

564 (9) Renforth, P. The Negative Emission Potential of Alkaline Materials. *Nat. Commun.*
565 **2019**, *10* (1). https://doi.org/10.1038/s41467-019-09475-5.

566 (10) Pan, S. Y.; Chen, Y. H.; Fan, L. S.; Kim, H.; Gao, X.; Ling, T. C.; Chiang, P. C.; Pei, S.
567 L.; Gu, G. CO2 Mineralization and Utilization by Alkaline Solid Wastes for Potential
568 Carbon Reduction. *Nat. Sustain.* **2020**, *3* (5), 399–405. https://doi.org/10.1038/s41893-
569 020-0486-9.

570 (11) Molahid, V. L. M.; Kusin, F. M.; Syed Hasan, S. N. M. Mineralogical and Chemical
571 Characterization of Mining Waste and Utilization for Carbon Sequestration through
572 Mineral Carbonation. *Environ. Geochem. Health* **2023**, *45* (7), 4439–4460.
573 https://doi.org/10.1007/s10653-023-01513-y.

574 (12) Lu, X.; Carroll, K. J.; Turvey, C. C.; Dipple, G. M. Rate and Capacity of Cation Release
575 from Ultramafic Mine Tailings for Carbon Capture and Storage. *Appl. Geochemistry*
576 **2022**, *140* (January), 105285. https://doi.org/10.1016/j.apgeochem.2022.105285.

577 (13) Bullock, L. A.; James, R. H.; Matter, J.; Renforth, P.; Teagle, D. A. H. Global Carbon
578 Dioxide Removal Potential of Waste Materials From Metal and Diamond Mining. *Front.*
579 *Clim.* **2021**, *3* (July), 1–12. https://doi.org/10.3389/fclim.2021.694175.

580 (14) Yip, C. K.; Lukey, G. C.; Provis, J. L.; van Deventer, J. S. J. Effect of Calcium Silicate
581 Sources on Geopolymerisation. *Cem. Concr. Res.* **2008**, *38* (4), 554–564.
582 https://doi.org/10.1016/j.cemconres.2007.11.001.

583 (15) Angulo, S. C.; Guilge, M. S.; Quarcioni, V. A.; Cincotto, M. A.; Nobre, T. R. S.;
584 Pöllmann, H. The Role of Calcium Silicates and Quicklime on the Reactivity of
585 Rehydrated Cements. *Constr. Build. Mater.* **2022**, *340* (November 2020).
586 https://doi.org/10.1016/j.conbuildmat.2022.127625.

587 (16) Wei, G.; Dong, B.; Fang, G.; Wang, Y. Understanding Reactive Amorphous Phases of
588 Fly Ash through the Acidolysis. *Cem. Concr. Compos.* **2023**, *140* (April), 105102.
589 https://doi.org/10.1016/j.cemconcomp.2023.105102.

590 (17) Pan, S. Y.; Chang, E. E.; Chiang, P. C. CO2 Capture by Accelerated Carbonation of
591 Alkaline Wastes: A Review on Its Principles and Applications. *Aerosol Air Qual. Res.*
592 **2012**, *12* (5), 770–791. https://doi.org/10.4209/aaqr.2012.06.0149.

593 (18) Hills, C. D.; Tripathi, N.; Carey, P. J. Mineralization Technology for Carbon Capture,
594 Utilization, and Storage. *Front. Energy Res.* **2020**, *8* (July), 1–14.
595 https://doi.org/10.3389/fenrg.2020.00142.

596 (19) Zevenhoven, R.; Eloneva, S.; Teir, S. Chemical Fixation of CO 2 in Carbonates : Routes
597 to Valuable Products and Long-Term Storage. **2006**, *115*, 73–79.
598 https://doi.org/10.1016/j.cattod.2006.02.020.

599 (20) Sanna, A.; Uibu, M.; Caramanna, G.; Kuusik, R.; Maroto-Valer, M. M. A Review of

Mineral Carbonation Technologies to Sequester CO2. *Chem. Soc. Rev.* **2014**, *43* (23), 8049–8080. https://doi.org/10.1039/c4cs00035h.

(21) Miller, Q. R. S.; Schaef, H. T.; Kaszuba, J. P.; Gadikota, G.; McGrail, B. P.; Rosso, K. M. Quantitative Review of Olivine Carbonation Kinetics: Reactivity Trends, Mechanistic Insights, and Research Frontiers. *Environ. Sci. Technol. Lett.* **2019**, *6* (8), 431–442. https://doi.org/10.1021/acs.estlett.9b00301.

(22) Monasterio-Guillot, L.; Di Lorenzo, F.; Ruiz-Agudo, E.; Rodriguez-Navarro, C. Reaction of Pseudowollastonite with Carbonate-Bearing Fluids: Implications for CO2 Mineral Sequestration. *Chem. Geol.* **2019**, *524* (December 2018), 158–173. https://doi.org/10.1016/j.chemgeo.2019.06.011.

(23) Romanov, V.; Soong, Y.; Carney, C.; Rush, G. E.; Nielsen, B.; O'Connor, W. Mineralization of Carbon Dioxide: A Literature Review. *ChemBioEng Rev.* **2015**, *2* (4), 231–256. https://doi.org/10.1002/cben.201500002.

(24) Min, Y.; Jun, Y. S. Wollastonite Carbonation in Water-Bearing Supercritical CO2: Effects of Water Saturation Conditions, Temperature, and Pressure. *Chem. Geol.* **2018**, *483* (January), 239–246. https://doi.org/10.1016/j.chemgeo.2018.01.012.

(25) Kashim, M. Z.; Tsegab, H.; Rahmani, O.; Abu Bakar, Z. A.; Aminpour, S. M. Reaction Mechanism of Wollastonite in Situ Mineral Carbonation for CO2Sequestration: Effects of Saline Conditions, Temperature, and Pressure. *ACS Omega* **2020**, *5* (45), 28942–28954. https://doi.org/10.1021/acsomega.0c02358.

(26) Pokrovsky, O. S.; Shirokova, L. S.; Bénézeth, P.; Schott, J.; Golubev, S. V. Effect of Organic Ligands and Heterotrophic Bacteria on Wollastonite Dissolution Kinetics. *Am. J. Sci.* **2009**, *309* (8), 731–772. https://doi.org/10.2475/08.2009.05.

(27) Scott, A.; Oze, C.; Shah, V.; Yang, N.; Shanks, B.; Cheeseman, C.; Marshall, A.; Watson, M. Transformation of Abundant Magnesium Silicate Minerals for Enhanced CO2 Sequestration. *Commun. Earth Environ.* **2021**, *2* (1), 1–6. https://doi.org/10.1038/s43247-021-00099-6.

(28) Bustillos, S.; Prentice, D.; La Plante, E. C.; Wang, B.; Sant, G.; Simonetti, D. Process Simulations Reveal the Carbon Dioxide Removal Potential of a Process That Mineralizes Industrial Waste Streams via an Ion Exchange-Based Regenerable PH Swing. *ACS Sustain. Chem. Eng.* **2022**, No. 2. https://doi.org/10.1021/acssuschemeng.2c00458.

(29) Kodama, S.; Nishimoto, T.; Yamamoto, N.; Yogo, K.; Yamada, K. Development of a New PH-Swing CO2 Mineralization Process with a Recyclable Reaction Solution. *Energy* **2008**, *33* (5), 776–784. https://doi.org/10.1016/j.energy.2008.01.005.

(30) Rim, G.; Wang, D.; Rayson, M.; Brent, G.; Park, A. H. A. Investigation on Abrasion versus Fragmentation of the Si-Rich Passivation Layer for Enhanced Carbon Mineralization via CO2 Partial Pressure Swing. *Ind. Eng. Chem. Res.* **2020**, *59* (14), 6517–6531. https://doi.org/10.1021/acs.iecr.9b07050.

(31) Ragipani, R.; Sreenivasan, K.; Anex, R. P.; Zhai, H.; Wang, B. Direct Air Capture and Sequestration of CO2by Accelerated Indirect Aqueous Mineral Carbonation under Ambient Conditions. *ACS Sustain. Chem. Eng.* **2022**, *10* (24), 7852–7861. https://doi.org/10.1021/acssuschemeng.1c07867.

(32) Baston, G. M. N.; Clacher, A. P.; Heath, T. G.; Hunter, F. M. I.; Smith, V.; Swanton, S. W. Calcium Silicate Hydrate (C-S-H) Gel Dissolution and PH Buffering in a Cementitious near Field. *Mineral. Mag.* **2012**, *76* (8), 3045–3053.

https://doi.org/10.1180/minmag.2012.076.8.20.

(33) Lakshtanov, L. Z.; Stipp, S. L. S. Interaction between Dissolved Silica and Calcium Carbonate: 1. Spontaneous Precipitation of Calcium Carbonate in the Presence of Dissolved Silica. *Geochim. Cosmochim. Acta* **2010**, *74* (9), 2655–2664. https://doi.org/10.1016/j.gca.2010.02.009.

(34) Kellermeier, M.; Gebauer, D.; Melero-García, E.; Drechsler, M.; Talmon, Y.; Kienle, L.; Cölfen, H.; García-Ruiz, J. M.; Kunz, W. Colloidal Stabilization of Calcium Carbonate Prenucleation Clusters with Silica. *Adv. Funct. Mater.* **2012**, *22* (20), 4301–4311. https://doi.org/10.1002/adfm.201200953.

(35) J.D.Rimstidt; H.L.Barnes. The Kinetics of Silica-Water Reactions. *Geochim. Cosmochim. Acta* **1980**, *44*, 1683–1699.

(36) Gal, A.; Weiner, S.; Addadi, L. The Stabilizing Effect of Silicate on Biogenic and Synthetic Amorphous Calcium Carbonate. *J. Am. Chem. Soc.* **2010**, *132* (38), 13208–13211. https://doi.org/10.1021/ja106883c.

(37) Zhai, H.; Wang, L.; Qin, L.; Zhang, W.; Putnis, C. V.; Putnis, A. Direct Observation of Simultaneous Immobilization of Cadmium and Arsenate at the Brushite-Fluid Interface. *Environ. Sci. Technol.* **2018**, *52* (6), 3493–3502. https://doi.org/10.1021/acs.est.7b06479.

(38) Zhai, H.; Bendikov, T.; Gal, A. Phase Separation of Oppositely Charged Polymers Regulates Bioinspired Silicification. *Angew. Chemie Int. Ed.* **2022**. https://doi.org/10.1002/ANIE.202115930.

(39) Zhai, H.; Wang, L.; Hövelmann, J.; Qin, L.; Zhang, W.; Putnis, C. V. Humic Acids Limit the Precipitation of Cadmium and Arsenate at the Brushite-Fluid Interface. *Environmental Science and Technology*. 2019, pp 194–202. https://doi.org/10.1021/acs.est.8b05584.

(40) Ho, H. J.; Iizuka, A.; Shibata, E.; Tomita, H.; Takano, K.; Endo, T. Utilization of CO2 in Direct Aqueous Carbonation of Concrete Fines Generated from Aggregate Recycling: Influences of the Solid–Liquid Ratio and CO2 Concentration. *J. Clean. Prod.* **2021**, *312* (June), 127832. https://doi.org/10.1016/j.jclepro.2021.127832.

(41) De Yoreo, J. J. Principles of Crystal Nucleation and Growth. *Rev. Mineral. Geochemistry* **2003**, *54* (1), 57–93. https://doi.org/10.2113/0540057.

(42) Min, Y.; Li, Q.; Voltolini, M.; Kneafsey, T.; Jun, Y. S. Wollastonite Carbonation in Water-Bearing Supercritical CO2: Effects of Particle Size. *Environ. Sci. Technol.* **2017**, *51* (21), 13044–13053. https://doi.org/10.1021/acs.est.7b04475.

(43) Liu, P.; Zhang, M.; Mo, L.; Zhong, J.; Xu, M.; Deng, M. Probe into Carbonation Mechanism of Steel Slag via FIB-TEM: The Roles of Various Mineral Phases. *Cem. Concr. Res.* **2022**, *162* (September), 106991. https://doi.org/10.1016/j.cemconres.2022.106991.

(44) Madrid, J. A.; Lanzón, M. Synthesis and Morphological Examination of High-Purity Ca(OH) 2 Nanoparticles Suitable to Consolidate Porous Surfaces. *Appl. Surf. Sci.* **2017**, *424*, 2–8. https://doi.org/10.1016/j.apsusc.2017.03.210.

(45) Min, Y.; Jun, Y. S. Wollastonite Carbonation in Water-Bearing Supercritical CO2: Effects of Water Saturation Conditions, Temperature, and Pressure. *Chem. Geol.* **2018**, *483* (October 2017), 239–246. https://doi.org/10.1016/j.chemgeo.2018.01.012.

(46) Wang, T.; Yi, Z.; Guo, R.; Huang, H.; Garcia, S.; Maroto-Valer, M. M. Particle

691 Carbonation Kinetics Models and Activation Methods under Mild Environment: The
692 Case of Calcium Silicate. *Chem. Eng. J.* **2021**, *423* (February), 130157.
693 https://doi.org/10.1016/j.cej.2021.130157.

694 (47) Wang, T.; Huang, H.; Hu, X.; Fang, M.; Luo, Z.; Guo, R. Accelerated Mineral
695 Carbonation Curing of Cement Paste for CO2 Sequestration and Enhanced Properties
696 of Blended Calcium Silicate. *Chem. Eng. J.* **2017**, *323*, 320–329.
697 https://doi.org/10.1016/j.cej.2017.03.157.

698 (48) Schott, J.; Pokrovsky, O. S.; Spalla, O.; Devreux, F.; Gloter, A.; Mielczarski, J. A.
699 Formation, Growth and Transformation of Leached Layers during Silicate Minerals
700 Dissolution: The Example of Wollastonite. *Geochim. Cosmochim. Acta* **2012**, *98*, 259–
701 281. https://doi.org/10.1016/j.gca.2012.09.030.

702 (49) Hellmann, R.; Cotte, S.; Cadel, E.; Malladi, S.; Karlsson, L. S.; Lozano-Perez, S.; Cabié,
703 M.; Seyeux, A. Nanometre-Scale Evidence for Interfacial Dissolution-Reprecipitation
704 Control of Silicate Glass Corrosion. *Nat. Mater.* **2015**, *14* (3), 307–311.
705 https://doi.org/10.1038/nmat4172.

706 (50) Geisler, T.; Dohmen, L.; Lenting, C.; Fritzsche, M. B. K. Real-Time in Situ
707 Observations of Reaction and Transport Phenomena during Silicate Glass Corrosion by
708 Fluid-Cell Raman Spectroscopy. *Nat. Mater.* **2019**, *18* (4), 342–348.
709 https://doi.org/10.1038/s41563-019-0293-8.

710 (51) Wu, J.; Zheng, H. Quantitative Measurement of the Concentration of Sodium Carbonate
711 in the System of Na2CO3-H2O by Raman Spectroscopy. *Chem. Geol.* **2010**, *273* (3–4),
712 267–271. https://doi.org/10.1016/j.chemgeo.2010.03.001.

713 (52) Tlili, M. M.; Amor, M. Ben; Gabrielli, C.; Joiret, S.; Maurin, G.; Rousseau, P. Study of
714 Electrochemical Deposition of CaCO[Sub 3] by In Situ Raman Spectroscopy. *J.*
715 *Electrochem. Soc.* **2003**, *150* (7), C485. https://doi.org/10.1149/1.1579483.

716 (53) Rusli, I. T.; Schrader, G. L.; Larson, M. A. Raman Spectroscopic Study of NaNO3
717 Solution System - Solute Clustering in Supersaturated Solutions. *J. Cryst. Growth* **1989**,
718 *97* (2), 345–351. https://doi.org/10.1016/0022-0248(89)90216-9.

719 (54) De Yoreo, J. J.; Gilbert, P. U. P. A.; Sommerdijk, N. A. J. M.; Penn, R. L.; Whitelam,
720 S.; Joester, D.; Zhang, H.; Rimer, J. D.; Navrotsky, A.; Banfield, J. F.; Wallace, A. F.;
721 Michel, F. M.; Meldrum, F. C.; Cölfen, H.; Dove, P. M. Crystallization by Particle
722 Attachment in Synthetic, Biogenic, and Geologic Environments. *Science (80-.).* **2015**,
723 *349* (6247). https://doi.org/10.1126/science.aaa6760.

724 (55) Annenkov, V. V.; Danilovtseva, E. N.; Pal'shin, V. A.; Verkhozina, O. N.; Zelinskiy, S.
725 N.; Krishnan, U. M. Silicic Acid Condensation under the Influence of Water-Soluble
726 Polymers: From Biology to New Materials. *RSC Adv.* **2017**, *7* (34), 20995–21027.
727 https://doi.org/10.1039/c7ra01310h.

728 (56) Kontrec, J.; Kralj, D.; Brečević, L.; Falini, G.; Fermani, S.; Noethig-Laslo, V.;
729 Mirosavljević, K. Incorporation of Inorganic Anions in Calcite. *Eur. J. Inorg. Chem.*
730 **2004**, No. 23, 4579–4585. https://doi.org/10.1002/ejic.200400268.

731 (57) Ben Amor, Y.; Bousselmi, L.; Bernard, M. C.; Tribollet, B. Nucleation-Growth Process
732 of Calcium Carbonate Electrodeposition in Artificial Water-Influence of the Sulfate
733 Ions. *J. Cryst. Growth* **2011**, *320* (1), 69–77.
734 https://doi.org/10.1016/j.jcrysgro.2011.02.005.

735 (58) Florides, G. A.; Christodoulides, P. Global Warming and Carbon Dioxide through
736 Sciences. *Environ. Int.* **2009**, *35* (2), 390–401.

https://doi.org/10.1016/j.envint.2008.07.007.